Anal. Chem. **2009,** *81,* 8923–8929

Bipolar Electrode Focusing: Simultaneous Concentration Enrichment and Separation in a Microfluidic Channel Containing a Bipolar Electrode

Derek R. Laws,[†] Dzmitry Hlushkou,[‡] Robbyn K. Perdue,[†] Ulrich Tallarek,*[,‡] and Richard M. Crooks*[,†]

Department of Chemistry and Biochemistry and Center for Electrochemistry, The University of Texas at Austin, 1 University Station, A5300, Austin, Texas 78712-0165, and Department of Chemistry, Philipps-Universität Marburg, Hans-Meerwein-Strasse, 35032 Marburg, Germany

A method for simultaneously concentrating and separating analytes in a buffer-filled microfluidic channel is reported. The approach is based on modulation of the local electric field within the channel and the corresponding opposition of electrophoretic and electroosmotic flow (EOF) velocities. Dye molecules having different electrophoretic mobilities are focused at different locations within the channel where concentration takes place. At least three species, all small dye molecules, can be simultaneously concentrated and separated, with localized enrichment factors up to ~600 achieved within 400 s. The enrichment zones affect the electric field profile, as evidenced by significant differences in focusing of single versus multiple analytes. The EOF could be modulated by modifying the channel walls with an appropriate polymer, and this had the effect of increasing both the enrichment factors and resolution of the separation. Numerical simulations provide insights into the underlying fundamental principles for the experimental findings.

We previously reported that modulation of the local electric field within a buffer-filled, microfluidic channel using a bipolar electrode (BPE) can lead to an analyte concentration of up to 45-fold.[1] Here, we expand upon this finding to show that the same general approach can be used to separate as well as concentrate analytes. Specifically, we show that solutions containing two or three fluorescent dyes, having different electrophoretic mobilities, can be separated and concentrated by up to 600-fold, often in less than 200 s. Simulations are presented to provide a better understanding of the experimental observations. Our findings are significant because of the simplicity and potential generality of the method and because of the interesting and previously unexplored underlying principles.

The appeal of concentration enrichment, or preconcentration, is that very low concentrations (often less than 1 nM) of analyte can be detected without resorting to ex situ sample preparation procedures. Some examples of techniques that accomplish concentration enrichment in microchannels and/or capillaries are methods based on electrophoresis,[2] electric field gradient focusing (EFGF),[3−6] dynamic field gradient focusing (DFGF),[6−8] isoelectric focusing,[9−11] isotachophoresis,[12,13] temperature gradient focusing,[6,14−17] electrokinetic supercharging,[18] and concentration polarization using nanopore membranes[19−21] or hydrogels.[22,23] Of particular interest to us are those methods that rely on electric field gradients for enrichment, the most well-recognized being EFGF. Originally, EFGF was used to describe a specific technique in which an electric field gradient is generated by applying a driving voltage across a tapered column (or channel).[5] The field

* To whom correspondence should be addressed. E-mail: crooks@cm.utexas.edu (R.M.C.); tallarek@staff.uni-marburg.de (U.T.).

[†] The University of Texas at Austin.

[‡] Philipps-Universität Marburg.

(1) Dhopeshwarkar, R.; Hlushkou, D.; Nguyen, M.; Tallarek, U.; Crooks, R. M. *J. Am. Chem. Soc.* **2008**, *130*, 10480–10481.

(2) Dolnik, V.; Liu, S.; Jovanovich, S. *Electrophoresis* **2000**, *21*, 41–54.

(3) Hlushkou, D.; Perdue, R. K.; Dhopeshwarkar, R.; Crooks, R. M.; Tallarek, U. *Lab Chip* **2009**, *9*, 1903–1913.

(4) Kelly, R. T.; Woolley, A. T. *J. Sep. Sci.* **2005**, *28*, 1985–1993.

(5) Koegler, W. S.; Ivory, C. F. *J. Chromatogr., A* **1996**, *726*, 229–236.

(6) Meighan, M. M.; Staton, S. J. R.; Hayes, M. A. *Electrophoresis* **2009**, *30*, 852–865.

(7) Huang, Z.; Ivory, C. F. *Anal. Chem.* **1999**, *71*, 1628–1632.

(8) Myers, P.; Bartle, K. D. *J. Chromatogr., A* **2004**, *1044*, 253–258.

(9) Sommer, G. J.; Hatch, A. V. *Electrophoresis* **2009**, *30*, 742–757.

(10) Shimura, K. *Electrophoresis* **2009**, *30*, 11–28.

(11) Hofmann, O.; Che, D.; Cruickshank, K. A.; Müller, U. R. *Anal. Chem.* **1999**, *71*, 678–686.

(12) Chen, L.; Prest, J. E.; Fielden, P. R.; Goddard, N. J.; Manz, A.; Day, P. J. R. *Lab Chip* **2006**, *6*, 474–487.

(13) Gebauer, P.; Mala, Z.; Bocek, P. *Electrophoresis* **2009**, *30*, 29–35.

(14) Shackman, J. G.; Munson, M. S.; Ross, D. *Anal. Bioanal. Chem.* **2007**, *387*, 155–158.

(15) Ross, D.; Locascio, L. E. *Anal. Chem.* **2002**, *74*, 2556–2564.

(16) Balss, K. M.; Vreeland, W. N.; Phinney, K. W.; Ross, D. *Anal. Chem.* **2004**, *76*, 7243–7249.

(17) Kim, S. M.; Sommer, G. J.; Burns, M. A.; Hasselbrink, E. F. *Anal. Chem.* **2006**, *78*, 8028–8035.

(18) Xu, Z.; Timerbaev, A. R.; Hirokawa, T. *J. Chromatogr., A* **2009**, *1216*, 660–670.

(19) Hahn, T.; O'Sullivan, C. K.; Drese, K. S. *Anal. Chem.* **2009**, *81*, 2904–2911.

(20) Long, Z.; Liu, D.; Ye, N.; Qin, J.; Lin, B. *Electrophoresis* **2006**, *27*, 4927–4934.

(21) Zhou, K.; Kovarik, M. L.; Jacobson, S. C. *J. Am. Chem. Soc.* **2008**, *130*, 8614–8616.

(22) Hlushkou, D.; Dhopeshwarkar, R.; Crooks, R. M.; Tallarek, U. *Lab Chip* **2008**, *8*, 1153–1162.

(23) Dhopeshwarkar, R.; Crooks, R. M.; Hlushkou, D.; Tallarek, U. *Anal. Chem.* **2008**, *80*, 1039–1048.

10.1021/ac901545y CCC: $40.75
Published on Web 09/30/2009

gradient is responsible for the migration of charged analytes in solution, and the velocity of migration is dependent on the electrophoretic mobility of the species employed. A constant opposing force, for example, hydrodynamic flow, stops analytes at specific positions where the two forces are equal (but opposite), yielding enriched analyte zones. Because a field gradient is used rather than a constant field, EFGF has the capability of both enriching and separating analytes that possess different mobilities. In our previous work, we demonstrated a new type of EFGF in microchannels containing a bipolar electrode (BPE).[1,3] The mechanism of field formation depends upon the electrochemical reactions at the edges of the BPE, with the constant opposing force being electroosmotic flow (EOF).

Other groups have used embedded electrodes to introduce electric field gradients for focusing purposes. For example, Lin et al. used a microfabricated Ti electrode to preconcentrate DNA,[24] although they describe the focusing mechanism in terms of a simple electrostatic attraction. Brahmasandra et al. reported DNA "compaction" between addressable microfabricated Pt electrodes in a microchannel[25] and investigated the effects of different electric field strengths on enrichment. Using DFGF, Huang and Ivory[7] demonstrated precise control over the shape of an electric field profile in a column using multiple individually addressable electrodes. This technique has since been adapted to microfluidic channels.[8] Perhaps the most pertinent work in relation to ours is that by Wei et al., who used a Pt BPE in a capillary to focus and separate various small fluorescent molecules.[26] Although the experimental arrangement was similar to ours, the focusing mechanism in this case was attributed to a pH gradient rather than an electric field gradient.

In the experiments reported here, a BPE was situated at the center of a microfluidic channel. When a sufficiently high driving voltage is applied across the buffer-filled channel, the BPE can provide a secondary current path. That is, in the vicinity of the BPE, current can be carried by both electrons (through the electrode) and ions (through the solution above the BPE). This results in complex ion transport due to the combined actions of electromigration (electrophoretic motion) and EOF, which in turn leads to an electric field gradient in the solution. The form of this gradient depends on a number of factors, including the driving voltage, the type and concentration of buffer, and the zeta-potential (ζ) of the microfluidic channel. We took advantage of the local electric field gradient to separate and concentrate up to three dye molecules having different electrophoretic mobilities. The initial concentrations of the dyes ranged from 0.1 to 0.8 μM, with final concentrations reaching up to 196 μM. Enrichment and baseline-resolved separation was achieved within 200 s.

EXPERIMENTAL SECTION

Chemicals. Poly(dimethylsiloxane) (PDMS) was prepared using a Sylgard 184 elastomer kit obtained from K. R. Anderson, Inc. (Morgan Hill, CA). Au-coated glass slides (100 nm thick, no adhesion layer) were purchased from EMF Corp. (Ithaca, NY). The three fluorescent tracers were 4,4-difluoro-1,3,5,7,8-pentamethyl-4-bora-3a,4a-diaza-*s*-indacene-2,6-disulfonic acid, disodium salt ($BODIPY^{2-}$, Invitrogen Corp., Carlsbad, CA), 8-methoxypyrene-1,3,6-trisulfonic acid ($MPTS^{3-}$, Anaspec, San Jose, CA), and 1,3,6,8-pyrene tetrasulfonic acid (PTS^{4-}, Fluka, Buchs, Switzerland). Pluronic F-108 was obtained from BASF (Ludwigshafen, Germany). TRIS buffer (pH 8.1) was prepared by dilution of a 1.0 M TRIS-HCl solution purchased from Fisher (Fair Lawn, NJ). Carbonate buffer (pH 10.0) was prepared by combining equimolar amounts of sodium carbonate and sodium bicarbonate purchased from Fisher. AZ 4620 photoresist and AZ 421 K developer were purchased from AZ Electronic Materials (Somerville, NJ). All chemicals were used as received. Deionized water having a resistivity greater than 18 MΩ cm was used for all experiments (Milli-Q gradient system, Millipore, Bedford, MA).

Microfluidic Device Fabrication. The driving electrodes and BPEs were deposited onto the glass base of the microfluidic device using standard photolithography techniques.[27] The driving electrodes consisted of microfabricated Au disks located at the bottoms of the two reservoirs. They were connected to a power supply via external contacts. In all cases, the Au BPEs were 0.5 mm × 1.0 mm × 100 nm. Two different channel lengths were used: the BPE was situated at the center of the 6 mm-long channels but offset by 3 mm toward the cathodic reservoir when 12 mm-long channels were employed.

Microchannels were fabricated in PDMS using a previously described replica molding procedure.[3,28] Specifically, channel masters having dimensions ($l \times w \times h$) of 6 mm × 100 μm × 22 μm or 12 mm × 100 μm × 22 μm were prepared on glass slides using two layers of AZ 4620 photoresist applied by spin coating at 2000 rpm. PDMS was poured over the channel masters in a Petri dish and allowed to cure for 2 h at 70°, at which point 4 mm diameter holes were punched at each end of the channel to serve as reservoirs. The PDMS was rinsed with ethanol, dried under N_2, and together with the glass slide supporting the Au electrodes, treated with an O_2 plasma (60 W, model PDC-32G, Harrick Scientific, Ossining, NY) for 30 s on the medium power setting. After joining the PDMS replica to the glass slide, the entire assembly was placed in a 70° oven for 7 min to promote irreversible bonding. A schematic representation of the entire system and an optical micrograph of the BPE region are provided in parts a and b of Figure 1, respectively.

Modification of the channel walls with Pluronic was carried out using a literature procedure,[29,30] but the modifier (Pluronic F-108) was present in either a 10.0 mM TRIS (pH 8.1) or carbonate (pH 10.0) solution (depending on the buffer to be used for the experiment) rather than phosphate buffer. Microfluidic devices were loaded with a 3.0 μM, buffered Pluronic solution and allowed to equilibrate for 20 h at 23 ± 2 °C. The channels were then thoroughly rinsed with buffer solution and used without further treatment. Electroosmotic mobility measurements were carried out on three different devices using the current monitoring

(24) Lin, Y. C.; Ho, H. C.; Tseng, C. K.; Hou, S. Q. J. *J. Micromech. Microeng.* **2001**, *11*, 189–194.
(25) Brahmasandra, S. N.; Ugaz, V. M.; Burke, D. T.; Mastrangelo, C. H.; Burns, M. A. *Electrophoresis* **2001**, *22*, 300–311.
(26) Wei, W.; Xue, G.; Yeung, E. S. *Anal. Chem.* **2002**, *74*, 934–940.
(27) Xia, Y.; Whitesides, G. M. *Angew. Chem., Int. Ed.* **1998**, *37*, 550–575.
(28) McDonald, J. C.; Duffy, D. C.; Anderson, J. R.; Chiu, D. T.; Hongkai, W.; Schueller, O. J. A.; Whitesides, G. M. *Electrophoresis* **2000**, *21*, 27–40.
(29) Hellmich, W.; Regtmeier, J.; Tu Duong, T.; Ros, R.; Anselmetti, A.; Ros, A. *Langmuir* **2005**, *21*, 7551–7557.
(30) Doherty, E. A. S.; Meagher, R. J.; Albarghouthi, M. N.; Barron, A. E. *Electrophoresis* **2003**, *24*, 34–54.

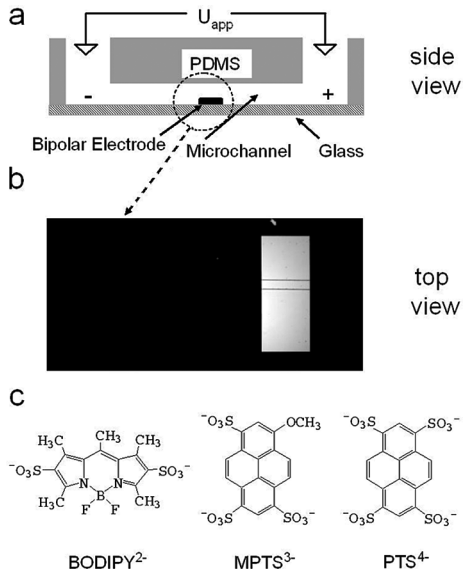

Figure 1. (a) Schematic illustration of the fluidic system used in these experiments, (b) optical micrograph of the BPE region of a typical device, and (c) structures of the anionic dyes (tracers).

method.[31] The results of six trials for each device were averaged to obtain the reported value.

Instrumentation and Data Acquisition. Fluorescence images were obtained using a Nikon AZ100 (Nikon Co., Tokyo, Japan) microscope equipped with a mercury lamp (Nikon) and a CCD camera (Cascade, Photometrics Ltd., Tucson, AZ). Micrographs were processed using V++ Precision Digital Imaging software (Digital Optics, Auckland, New Zealand), and the movies were generated with a custom program allowing for capture of multiple consecutive frames. Images were captured using 1×1 binning with 512×290 pixels and a 100 ms exposure time. Movie images were captured using the same parameters and a rate of either 1 or 2 frame(s)/s. An appropriate, fixed grayscale was applied to all movies following acquisition. Fluorescence intensities for calibration curves were obtained using a function that averages intensities of all pixels along one axis of the region of interest. Fluorescence intensities of concentrated analytes were obtained using a maximum function, which gives the maximum intensity values along one axis of the region of interest. All values reported are background subtracted. Enrichment factors were calculated by determining the enriched dye concentration using calibration curves and then dividing this value by the original dye concentration.

Computer Simulations. We present below a brief description of the theoretical formulation and numerical approach used for the computer simulations. This description is based on our earlier publications.[1,3]

Governing Physical Equations. The basic equations governing the physical phenomena in the system are the Nernst−Planck (eq 1), Poisson (eq 2), and Navier−Stokes (eq 3) equations.

$$\frac{\partial c_i}{\partial t} = \nabla \cdot (D_i \nabla c_i) - \frac{z_i F}{RT} \nabla \cdot (D_i \nabla \phi) - c_i \nabla \cdot \mathbf{v} + r_i \qquad (1)$$

$$\nabla^2 \phi = -\frac{F}{\varepsilon_0 \varepsilon_r} \sum_i z_i c_i \qquad (2)$$

$$\rho\left(\frac{\partial \mathbf{v}}{\partial t} + \mathbf{v} \cdot \nabla \mathbf{v}\right) = -\nabla p + \mu \nabla^2 \mathbf{v} - F(\nabla \phi) \sum_i z_i c_i \qquad (3)$$

Here, c_i is the molar concentration of species i; D_i and z_i are its diffusion coefficient and valency, respectively; ϕ is the local electric potential; F, R, and T represent the Faraday constant, molar gas constant, and absolute temperature, respectively; $\mathbf{v}$ is the flow velocity; r_i is the homogeneous reaction term for species i; ε_0 and ε_r are the vacuum permittivity and dielectric constant; ρ and μ are the mass density and dynamic viscosity of the liquid; and p is hydrostatic pressure. The kinetics of the assumed faradaic and buffer reactions as well as the diffusion coefficients and charges of the species used in the simulations are provided in the Supporting Information.

Numerical Methods. In all simulations, the BPE was 500 μm wide and situated at the center of the channel. To reduce computation time, only 1.5 mm of the channel length used in the experiments was modeled.

The mathematical model of the processes in the system was implemented as an iterative model based on discrete spatiotemporal schemes optimized for parallel computations. In particular, for the solution of the Navier−Stokes, Poisson, and Nernst−Planck equations, the lattice-Boltzmann approach[32] and the numerical approaches described by Warren[33] and by Capuani et al.[34] were employed. In all numerical schemes, a time step of 1×10^{-5} s and a space step of 10^{-6} m were used. At each time step, the Poisson equation was solved 10 times with an under-relaxation factor of 0.25 to ensure numerical stability. A single simulation required ~16 h using 40 processors of an SGI Altix 4700 supercomputer to analyze the temporal behavior of the system for 50 s.

RESULTS AND DISCUSSION

The structures of the three fluorescent dyes used as tracers in these experiments are provided in Figure 1c. These three sulfonated dyes are relatively insensitive to pH due to their low pK_a values,[35] which eliminates contributions to enrichment and separation resulting from pH gradients within the channel. Here, we used buffer concentrations ranging from 1 to 5 mM, but we have had success in single-analyte concentration experiments with buffer concentrations of up to 50 mM. The disadvantage of higher concentrations is the likelihood of bubble formation, which may be controlled to some extent by using lower driving voltages.

TRIS Buffer System. When an applied driving voltage (U_{app}, Figure 1a) of 40 V (E_{app} = 6.67 kV/m) is applied across a microchannel containing 0.1 μM $BODIPY^{2-}$ and 0.2 μM $MPTS^{3-}$ in 5.0 mM TRIS buffer, both analytes exhibit concentration enrichment at the same location close to the right (cathodic) edge of the BPE. However, after ~20 s, two distinct bands begin to emerge, and after 200 s (Figure 2a), the bands fully resolve. In Figure 2a, the band closest to the electrode is $BODIPY^{2-}$ and the other is $MPTS^{3-}$, as determined by using two different fluorescent filters (see description of filter sets

(31) Huang, X.; Gordon, M. J.; Zare, R. N. *Anal. Chem.* **1988**, *60*, 1837–1838.
(32) Higuera, F. J.; Jiménez, J. *Europhys. Lett.* **1989**, *9*, 663–668.
(33) Warren, P. B. *Int. J. Mod. Phys. C* **1997**, *8*, 889–898.
(34) Capuani, F.; Pagonabarraga, I.; Frenkel, D. *J. Chem. Phys.* **2004**, *121*, 973–986.
(35) Merz, K. M., Jr.; Murcko, M. A.; Kollmans, P. A. *J. Am. Chem. Soc.* **1991**, *113*, 4484–4490.

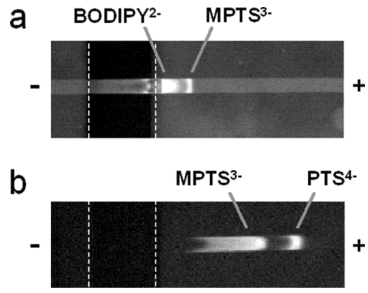

Figure 2. Fluorescence micrographs (top views) demonstrating separation of anionic dyes in 5.0 mM TRIS. (a) $BODIPY^{2-}$ and $MPTS^{3-}$ 200 s after application of $U_{app} = 40$ V (XF115-2). (b) $MPTS^{3-}$ and PTS^{4-} 400 s after application of $U_{app} = 60$ V (XF02-2). Filter sets used for data collection are given in parentheses, and additional information is provided in the Supporting Information. Dashed lines indicate the positions of the edges of the BPE. The channel is 6 mm long.

in the Supporting Information). At 200 s, the enrichment factors for $BODIPY^{2-}$ and $MPTS^{3-}$ are 30 and 150, respectively. The entire time course of this separation is provided in Movie S1 (Supporting Information). When the same experiment is carried out, but with just the individual dyes present, the enrichment factors are about 60 and 200, respectively (Supporting Information, Figure S1). Clearly, the magnitude and location of enrichment depends on the number and identity of the analytes. This is a consequence of the time-dependent modulation of the field driven by localized enrichment.

Figure 2b is a fluorescence micrograph of a solution containing 0.2 μM $MPTS^{3-}$ and 0.2 μM PTS^{4-} in 5.0 mM TRIS, which was obtained 400 s after application of the driving voltage ($U_{app} =$ 60 V). Compared to the $BODIPY^{2-}$ and $MPTS^{3-}$ separation described in the previous paragraph, a higher U_{app} and a longer time ($U_{app} = 40$ V and $t = 200$ s) were required to achieve a fully resolved separation. In the present case, it was not possible to experimentally verify the identities of the analyte bands due to the similarities in the absorption and emission spectra of $MPTS^{3-}$ and PTS^{4-}. However, simulations discussed later suggest that the band closer to the BPE is $MPTS^{3-}$ and that the other is PTS^{4-}. Enrichment factors for $MPTS^{3-}$ and PTS^{4-} were 70 and 490, respectively, after 400 s.

To assist with interpretation of the experimental results, mass-transfer simulations were carried out for $BODIPY^{2-}$ and $MPTS^{3-}$ in pH 8.1, 5.0 mM TRIS buffer. As discussed in the Experimental Section, the simulations were based on numerical resolution of the coupled Navier−Stokes, Nernst−Planck, and Poisson equations, taking into account faradaic reactions at the edges of the BPE and inherent reactions of each buffer system.

Figure 3 illustrates the combined enrichment/separation events simulated for $BODIPY^{2-}$ and $MPTS^{3-}$. Figure 3a shows the axial distribution of the enrichment factors. As in the experiments, both analytes were concentrated in the anodic segment of the microchannel.

The presence of the BPE results in a local depletion of electrolyte ions and a lower conductivity of the solution directly to the right of the BPE.[1] The implication of these results is that tracer molecules coming from the anodic reservoir encounter an increasing electrophoretic force in the opposite direction (back toward the anodic reservoir) as they approach the BPE due to the field gradient. At certain axial positions, the two counter-

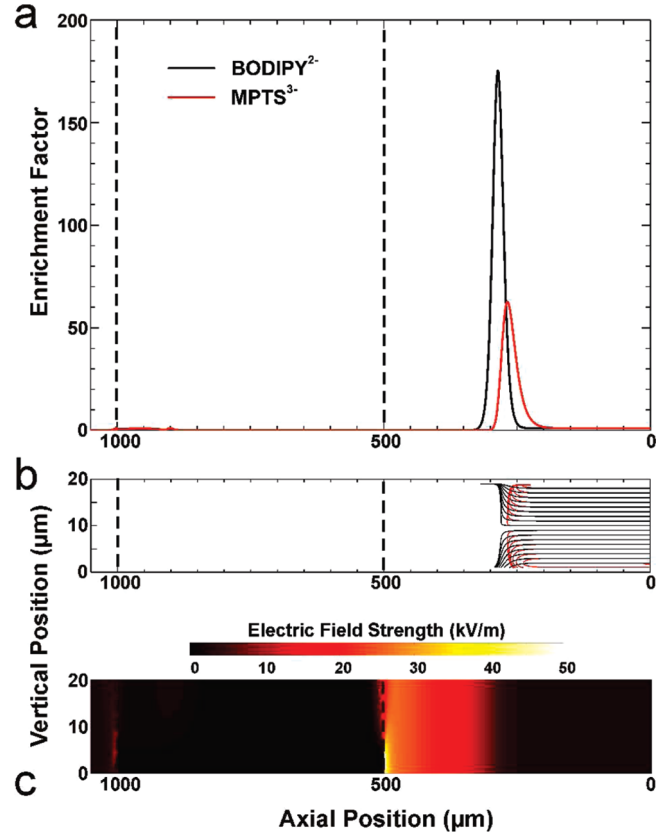

Figure 3. (a) Axial distribution of the simulated enrichment factors in 5.0 mM TRIS buffer (pH 8.1) with $\zeta = -85$ mV. (b) Analyte-specific transport streamlines ($E_{app} = 6.67$ kV/m). (c) Distribution of the axial electric field strength. The BPE is located at the vertical position of 0 μm and at the axial position between 500 and 1000 μm. The simulated channel is 1.5 mm long.

directional components (anodic electrophoresis vs cathodic advective flow) are balanced. When this happens, tracer molecules become quasi-stationary and locally enriched, with enriched zones being separated because $BODIPY^{2-}$ and $MPTS^{3-}$ have different mobilities.

Figure 3b shows the transport pathways followed by $BODIPY^{2-}$ and $MPTS^{3-}$ in the vicinity of the BPE. These streamlines, which are determined as the local sum of electrophoretic and advective components, can be considered as the specific transport trajectories for each analyte entering the microchannel. The electrophoretic component results from electrostatic interactions of the charged analytes with the local electric field, while the advective component is a combined result of the EOF, characterized by the ζ of the microchannel walls, and local pressure-driven flow. Figure 3c is the simulated electric field distribution for a total applied field of 6.67 kV/m. It is significant that the field is strongest at the cathodic edge of the BPE (axial position of 500 μm) and declines with distance over the height and length of the microchannel.

It is important to note that although the enrichment factors for simulation and experiment do not match quantitatively, the agreement is reasonable considering simplifications and assumptions involved in the numerical model. For instance, we assumed stationary, time-independent concentration boundary conditions at the microchannel inlet (i.e., in the anodic reservoir). In fact, the actual spatiotemporal distribution of concentrations in the

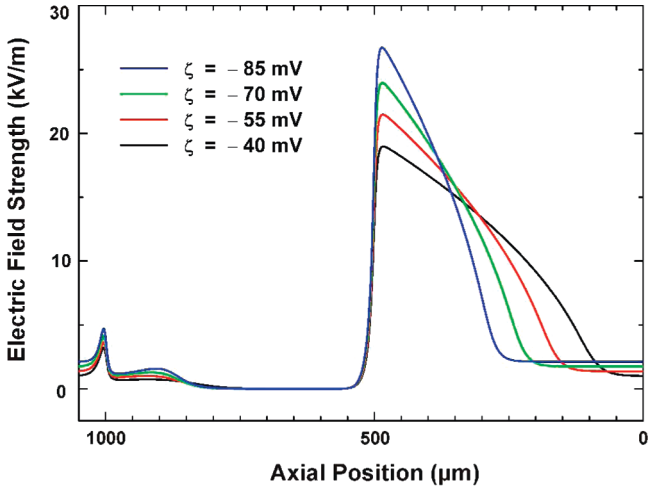

Figure 4. Axial distribution of the simulated electric field strength in 5.0 mM TRIS buffer (pH 8.1) for the values of ζ of the microchannel wall indicated in the legend. The BPE is located at the axial position between 500 and 1000 μm. The simulated channel is 1.5 mm long.

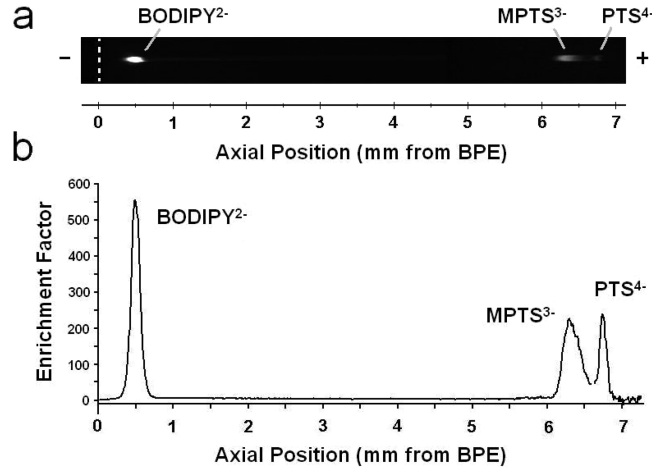

Figure 5. (a) Fluorescence micrograph (top view) showing separation of $BODIPY^{2-}$, $MPTS^{3-}$, and PTS^{4-} in 5.0 mM TRIS 200 s after application of $U_{app} = 40$ V (XF115-2 and XF02-2 filter sets overlaid, see Supporting Information) in a 12 mm-long, Pluronic-modified channel. (b) Plot of enrichment factor vs axial location corresponding to part a.

reservoirs is rather complicated. The dominating transport mechanisms for the charged analytes in the reservoir are diffusion and electrophoresis. By application of a potential bias, negatively charged species in the anodic reservoir are forced to migrate toward the anode. This redistribution can result in the formation of a diluted zone (as compared to the initial, uniform buffer concentration in the reservoir) near the microchannel inlet. Therefore, a side-by-side comparison between experiment and simulation requires that the macroscale reservoirs be included in the simulated system. This was not possible in the present case due to limited computational resources.

Another assumption used for the simulations is that the ζ of the microchannel walls is constant and not influenced by changes in local solution pH and ionic strength. Indeed, dynamic changes in the value of ζ can affect the electric field strength profile in the anodic segment of the microchannel. This has been resolved by our simulations and is further illustrated in Figure 4 where we present distributions of local field strength for $\zeta = -40$, -55, -70, and -85 mV. The higher the ζ, the steeper and narrower the field gradient that develops between the BPE and anodic reservoir. Of course, the situation becomes more complex when ζ varies as a function of axial position.

The next set of experiments involved separation and concentration of three analytes simultaneously: $BODIPY^{2-}$, $MPTS^{3-}$, and PTS^{4-}. However, the device configuration and range of experimental parameters that were successfully used for the two-analyte separation resolved just two of the three bands in the present case. Accordingly, two changes were made to the experimental design. First, additional distance was provided for the separation by increasing the channel length from 6 to 12 mm and moving the BPE from the center of the channel toward the cathodic reservoir by 3 mm. Although the electric field gradient is located only near the edge of the BPE, the constant electric field in other locations results in the analytes migrating at different velocities. Second, the interior walls of the channels were modified with Pluronic to minimize the EOF.[29,30] This resulted in a decrease of the EOF by ~60%. The decrease in EOF results in a lengthening of the electric field gradient (Figure 4), which provides more space for analytes to separate. This is important, because the enrichment zones represent regions of high solution conductivity. This eliminates the field gradient in these regions of the microchannel, thereby minimizing the separation capacity in these regions.

When a driving voltage of $U_{app} = 90$ V ($E_{app} = 7.5$ kV/m) is applied across a 12 mm-long, Pluronic-treated channel containing 5.0 mM TRIS, 0.1 μM $BODIPY^{2-}$, 0.4 μM $MPTS^{3-}$, and 0.8 μM PTS^{4-}, three enriched zones are observed after 100 s. After 200 s, the three analyte zones are resolved (Figure 5 and Movie S2 in the Supporting Information). The enrichment factors for the di-, tri-, and tetraanion at 200 s are 560, 225, and 245, respectively. It is likely that separations of more than three analytes can be accomplished using this approach, although the electric field profile of the system is affected by each added analyte, and therefore predicting the location of the separated bands is not straightforward.

Carbonate Buffer System. In the previous section, we described BPE focusing carried out in TRIS buffer. To better understand how the buffer affects both separation and enrichment, we now turn our attention to pH 10.0 carbonate buffer.[1,3] For these experiments it was necessary to use a lower buffer concentration (1.0 mM rather than the 5.0 mM used for the TRIS system), because at higher concentrations bubbles formed on the BPE. When a driving voltage of $U_{app} = 40$ V is applied across a microchannel containing 0.1 μM $BODIPY^{2-}$ and 0.2 μM $MPTS^{3-}$ in 1.0 mM carbonate buffer, two distinct bands are observed after 200 s (Figure 6a). The top frame of this figure shows the concentrated $BODIPY^{2-}$ band and the lower frame, which was taken using a different filter after a delay of 3 s (see Supporting Information for details), shows the concentrated $MPTS^{3-}$ band. Movie S3 in the Supporting Information shows the time course of this experiment. At 200 s, enrichment factors for $BODIPY^{2-}$ and $MPTS^{3-}$ are 35 and 180, respectively. The most notable difference between the experiments carried out in carbonate and TRIS buffers is that anions concentrate either directly over the BPE or even in the cathodic segment of the

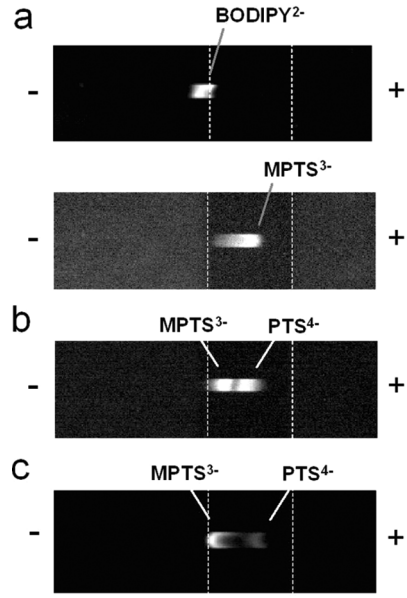

Figure 6. Fluorescence micrographs (top views) demonstrating separation of anionic dyes in 1.0 mM carbonate buffer. (a) $BODIPY^{2-}$ and $MPTS^{3-}$ 200 s after application of U_{app} = 40 V (top: XF115-2, bottom: XF02-2, 3 s later). (b) $MPTS^{3-}$ and PTS^{4-} 400 s after application of U_{app} = 40 V (XF02-2). (c) Same as part b but with a Pluronic-modified channel. Filter sets used for data collection are given in parentheses and additional information is provided in the Supporting Information. The dashed lines indicate the positions of the edges of the BPE.

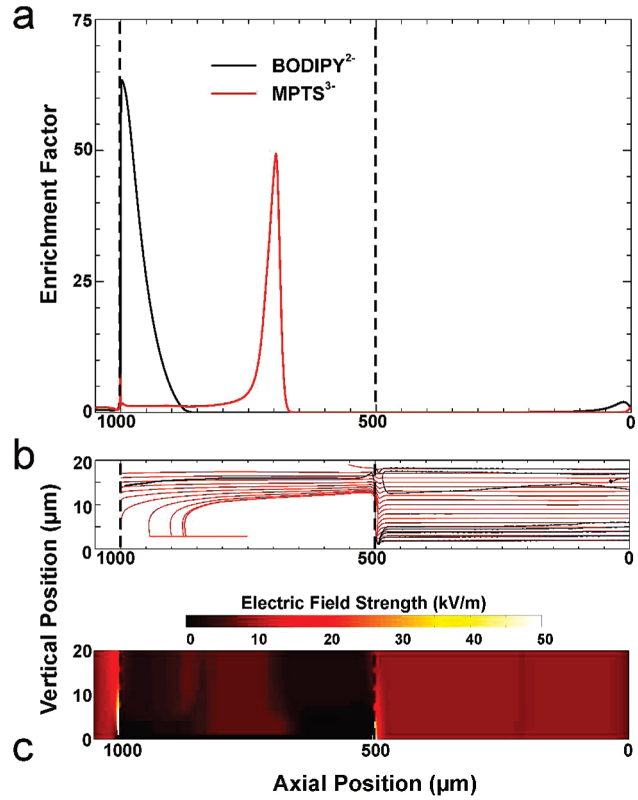

Figure 7. (a) Axial distribution of the simulated enrichment factors in 1.0 mM carbonate buffer (pH 10.0) with $\zeta = -100$ mV. (b) Analyte-specific transport streamlines (E_{app} = 6.67 kV/m). (c) Distribution of axial electric field strength. The BPE is located at the vertical position of 0 μm and at the axial position between 500 and 1000 μm. The simulated channel is 1.5 mm long.

microchannel in carbonate buffer. The reason for this behavior is discussed later in the context of the simulations. In Figure 6a and Movie S3 in the Supporting Information, a second, very weak $BODIPY^{2-}$ band may be observed over the right edge of the BPE. Although we cannot say with certainty why $BODIPY^{2-}$ concentrates at this location, we presume it is due to the complex nature of the electric field in the carbonate buffer (Figure 7c) that results in multiple potential enrichment zones.

When a driving voltage of U_{app} = 40 V is applied across a microchannel containing 0.2 μM $MPTS^{3-}$ and 0.2 μM PTS^{4-} in 1.0 mM carbonate buffer, two bands are observed after 400 s (Figure 6b). Enrichment occurs directly over the BPE. The enrichment factors for $MPTS^{3-}$ and PTS^{4-} are 430 and 205, respectively, at 400 s. The same experiment (U_{app} = 40 V) was conducted using a Pluronic-modified channel, and the results, which are shown in Figure 6c, indicate that the decrease in EOF leads to improved resolution. Moreover, substantial enrichment and separation occur within just 150 s. In this experiment, the enrichment factors for $MPTS^{3-}$ and PTS^{4-} were 510 and 290, respectively, at 400 s.

Simulations in carbonate buffer reveal important differences compared to the results obtained for the TRIS system. In carbonate, the electric field gradient formed in the anodic segment of the microchannel does not provide a sufficient electrophoretic force to overcome the cathodic EOF throughout the entire height of the channel (Figure 7b). As a result, both analytes can pass the anodic channel segment and enter the region above the BPE through the upper part of the microchannel (vertical position >12 μm). The region above the BPE is characterized by a very low electric field strength along the axial direction, and analyte molecules are transported through this region mainly from right to left by the advective flow of the electrolyte solution.

In carbonate buffer (but not in TRIS) a transverse electric field exists above the BPE (compare Figure 7c to Figure 3c). This transverse field deflects tracer molecules toward the surface of the BPE; the magnitude of the transverse electrophoretic force is determined by the mobility of the tracer. For example, this transverse force is sufficiently strong to move $MPTS^{3-}$ toward the surface of the BPE (Figure 7b). The thin boundary layer of electrolyte solution adjoining this surface is characterized by a very low flow velocity due to the fact that flow in this region is pressure-driven and satisfies the no-slip velocity boundary condition at the solid−liquid interface. Therefore, $MPTS^{3-}$ that reaches the surface of the BPE can be transported electrophoretically in the opposite direction of the bulk flow (i.e., from left to right) even by the very weak axial electric field. $BODIPY^{2-}$ molecules experience a weaker transverse electrophoretic force in the BPE segment and therefore do not reach its surface (Figure 7b). Instead, $BODIPY^{2-}$ is transported through the region above the electrode by the advective flow of the bulk solution and arrives at a position where a second electric field gradient has formed. The electrophoretic force here is sufficiently large to allow concentration close to the anodic edge of the BPE (axial position of 1000 μm), and the field here persists along the entire channel height so that $BODIPY^{2-}$ molecules cannot penetrate into the cathodic channel segment.

The differences in enrichment and separation behavior of the TRIS and carbonate buffer systems can be related primarily to the transport pathways followed by the analytes. This is illustrated in Figure 3b for the TRIS system and in Figure 7b for the carbonate system. In the TRIS system, the electric field strength near the cathodic edge of the BPE is high along the entire height of the channel. Anions encounter the steadily increasing field and eventually become stationary due to the opposing electrophoretic force and EOF. The carbonate system is somewhat different because analytes are able to pass through the low conductivity region higher in the channel (>12 μm) and enter the BPE segment before encountering another region having electric field gradients. These latter gradients are strong enough to counteract the advective flow and result in concentration enrichment above the electrode.

SUMMARY AND CONCLUSIONS

A BPE enclosed in a microfluidic channel controls the local electric field, generating electric field gradients in its vicinity. This leads to local differences in the transport properties of charged analytes possessing dissimilar electrophoretic mobilities, and hence simultaneous concentration enrichment and separation is possible. Because of the transport properties of the background ionic species, the resulting field gradients depend on the particular buffer system, providing flexibility for optimizing separation and concentration enrichment for different analytes. We demonstrated that at least three analytes may be simultaneously enriched and separated in less than 200 s using this technique. The benefit of this method over other simultaneous enrichment and separation techniques is its simplicity and its potential for generality and versatility. Here, the only requirements are a simple PDMS microchannel, a small strip of metal or other conductive material, and a power supply. Such a system could easily be incorporated as a component in an integrated microfluidic device. Moreover, the simplicity of this approach lends itself to nanofluidic applications. Although not discussed here, the locations of enriched bands are easily manipulated using pressure driven flow or slight voltage changes, so that a controlled delivery of analyte might be accomplished either by forcing the band to the end of the channel or by incorporating cross channels. Experiments describing these results will be reported in due course.

ACKNOWLEDGMENT

We gratefully acknowledge the U.S. Department of Energy, Office of Basic Energy Sciences (Contract No. DE-FG02-06ER15758) for support of this work. We also thank the Robert A. Welch Foundation (Grant F-0032). Simulations were run at the "Leibniz-Rechenzentrum der Bayerischen Akademie der Wissenschaften" (Garching, Germany), supported by Project HLRB pr26wo. This report is based in part upon work supported under a National Science Foundation Graduate Research Fellowship to R.K.P.

SUPPORTING INFORMATION AVAILABLE

Micrographs showing experimental results using single analytes, three movies (MPG format) showing the entire separation experiments represented by Figures 2, 5, and 6, a description of microscopy filters used, and a description of the chemical reactions used for simulations of the TRIS and carbonate systems. This material is available free of charge via the Internet at http://pubs.acs.org.

Received for review July 12, 2009. Accepted September 14, 2009.

AC901545Y